PERGAMON

International Journal of Heat and Mass Transfer 43 (2000) 2395–2404

International Journal of HEAT and MASS TRANSFER

www.elsevier.com/locate/ijhmt

Flow and heat transfer characteristics of a two-dimensional oblique wall attaching offset jet

Heung Bok Song[a], Soon Hyun Yoon[b], Dae Hee Lee[c,*]

[a]*Korea Electric Power Research Institute, Taejon, South Korea*
[b]*Department of Mechanical Engineering, Pusan National University, Pusan 609-735, South Korea*
[c]*School of Mechanical and Automotive Engineering, Inje University, Kimhae 621-749, South Korea*

Received 21 August 1998; received in revised form 23 April 1999

Abstract

Turbulent flow and heat transfer characteristics of a two-dimensional oblique wall attaching offset jet were experimentally investigated. The local Nusselt number distributions were measured using liquid crystal as a temperature sensor. The jet mean velocity, turbulent intensity and wall static pressure coefficient profiles were measured for the jet Reynolds number, $Re = 53{,}200$, the offset ratio (H/D) from 2.5 to 10, and the oblique angle, α from 0° to 40°. It is observed that the time-averaged reattachment point nearly coincides with the maximum Nusselt number point for all oblique angles, but the maximum pressure point does only for $\alpha = 0^\circ$. The decay of the maximum jet velocity in the streamwise direction is found to obey the conventional $-1/2$ power law of the wall attaching offset jet for $\alpha \leq 30^\circ$. The reattachment length and maximum pressure point are well correlated with offset ratio and oblique angle. The correlations between the maximum Nusselt number and Reynolds number for all oblique angles tested are presented.

Keywords: Oblique wall attaching offset jet; Liquid crystal; Nusselt number; Coanda effect; Gold film Intrex

1. Introduction

The Oblique Wall Attaching Offset Jet (OWAOJ) is a two-dimensional slot jet issued into quiescent surroundings above an inclined plate. As depicted in a schematic diagram of the OWAOJ in Fig. 1, when the jet discharges from the nozzle, the so-called "coanda effect" causes the jet to deflect towards the wall boundary and reattach to the plate wall. The jet redevelops in the wall jet region after its reattachment to the wall.

OWAOJ is frequently encountered in numerous industrial applications such as the cooling of a combustion chamber wall in a gas turbine, an air deflector as a circulation controller, an automobile demister, and a moisture remover in the car washer. In spite of its wide applications to practical engineering problems, however, no previous research on the OWAOJ has been found in the literature search.

In the mean time, numerous studies on the wall attaching offset jet (WAOJ) have been performed. Borque and Newmann [1] and Sawyer [2] studied the mean flow characteristics of the WAOJ. Hoch and Jiji [3] numerically predicted the jet trajectory, jet reattachment length, wall pressure distribution, and maximum axial velocity decay. Pelfray and Liburdy [4] provided the mean velocity and turbulent intensity profiles in the recirculation and impin-

* Corresponding author.

0017-9310/00/$ - see front matter
PII: S0017-9310(99)00312-9

Nomenclature

C_{Pw}	wall static pressure coefficient ($=(P_W-P_\infty)1/2\rho U_J^2$)
D	nozzle width
f	gold-coating uniformity on the Intrex surface
H	distance from the wall to the lower nozzle edge
h	convection heat transfer coefficient
k	thermal conductivity of air
Nu	local Nusselt number, hD/k
Nu_{max}	maximum Nusselt number
P_W	wall static pressure
P_∞	atmospheric pressure
q	heat flux
Re	jet Reynolds number (based on the nozzle width, D)
T	temperature
U	axial mean velocity
U_J	jet mean velocity at the nozzle exit
U_m	maximum axial mean velocity
u', v', w'	r.m.s. values of the velocity fluctuation components
X, Y	horizontal and vertical coordinate
X^α, Y^α	horizontal and vertical coordinate along the inclined wall
$X^\alpha_{Nu_{max}}$	maximum Nusselt number position
X^α_R	reattachment distance
$X^\alpha_{cp_{max}}$	maximum pressure position
$Y_{1/2m}$	upper jet spread

Greek symbols

α	oblique angle
ε	emissivity of the liquid crystal and black paint coated on the plate surface
ρ	density of air
γ	forward flow fraction
σ	Stefan–Boltzmann constant

Subscripts

a	ambient
c	conduction
cr	critical
J	jet
v	convection
W	oblique wall

gement regions. Yoon et al. [5] presented the detailed flow data in the entire region of the WAOJ. Kumada et al. [6] measured the mass transfer coefficients in the WAOJ using the naphthalene sublimation technique. Hoch and Jiji [7], and Holland and Liburdy [8] studied the thermal characteristics of the heated WAOJ, and the temperature and energy distributions of the heated WAOJ, respectively. Most recently, Kim et al. [9] investigated the flow and heat transfer characteristics of the WAOJ and found that a dividing streamline of the jet unstably reattaches in the impingement region. They also found that the jet reattachment point nearly coincides with the maximum Nusselt number position and presented correlations between the local Nusselt number distributions and Reynolds number, offset ratio, and streamwise length.

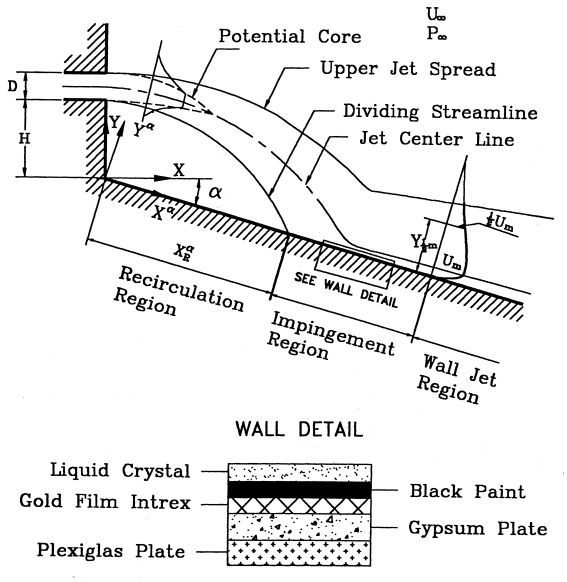

Fig. 1. Schematic diagram of the oblique wall attaching offset jet flow experiment.

In the present study, the mean velocities, wall static pressure coefficients, and local heat transfer coefficients in the entire region of the OWAOJ are measured by employing a split film probe and thermochromic liquid crystal. The Reynolds number, Re ranges from 17,700 to 53,200, the offset ratio, H/D from 2.5 to 10, the oblique angle, α from 0° to 40°. This research is an extension of the previous work by Kim et al. [9] in that it investigates the effect of the oblique angle on the flow and heat transfer characteristics of the two-dimensional WAOJ. The purpose of the present research is to obtain good quality data with the well-defined thermal wall boundary condition and inlet flow conditions, which the people developing the compu-

tational code for turbulent heat transfer prediction can use as a reliable source.

2. Experimental apparatus

Measurements are made in a low speed blow-down wind tunnel. Air is moved by 5 HP centrifugal fan and an inverter controls the fan speed. The wind tunnel consists of a diffuser, a plenum chamber and a contraction nozzle. A size of the plenum chamber is 300 mm × 300 mm and a size of the nozzle is 300 mm × 25 mm, resulting in an aspect ratio of 12. The test plate on which the discharged jet attaches is made up of 1800 mm × 300 mm × 10 mm Plexiglas. The test plate surface is heated with gold film Intrex (a 0.13 mm thick polyester substrate sheet on which an approximately 20 Å thick gold-coating is applied) by passing a D.C. current, which creates a uniform heat flux boundary condition on the plate surface.

The liquid crystal used in this experiment is "R35C3W", microencapsulated thermochromic liquid crystal. Since the actual color image of liquid crystal is affected by the factors such as the thickness of liquid crystal, the angle and distance of the light illuminating the liquid crystal coated surface, a careful color calibration has to be carried out under the particular conditions and later the experiments are carried out under the same conditions as those for the calibration.

For the calibration purpose, a 170 mm × 75 mm × 50 mm aluminum block is used through the top of which a 100 W cartridge heater is embedded, while the bottom 50 mm of the block is immersed in the constant temperature water bath maintaining to within $\pm 0.01^{\circ}$C of the set temperature, generating a linear temperature gradient along the length of the aluminum block. A layer of black paint and liquid crystal to be calibrated is air-brushed on the aluminum block surface. To measure the surface temperature, eight calibrated thermocouples fed through the back of the block are used and their junctions are flush with the liquid crystal coated surface. It should be noted that the sides and back of the block are covered with urethane foam insulation to minimize the conduction heat loss. The color distribution on the block is then recorded and processed by a digital color image processing system, producing a color/temperature calibration result with hue value as a function of temperature. The digital color image processing system consists of a color video camera (SAMSUNG/SV-F12), a color frame grabber (DARIM/Video-Catcher), and Pentium-PC.

Now, the flow measurements are made for $Re = 53{,}200$, $H/D = 5.0$, $\alpha = 0^{\circ}$ to 40°. Heat transfer measurements are made for $Re = 17{,}700$ to $53{,}200$, $H/D = 2.5$ and 5.0, and $\alpha = 0^{\circ}$ to 40°. Both the flow and the heat transfer measurements are carried out along the centerline of the plate in the longitudinal direction to insure the two-dimensional jet flow assumption. It is observed that liquid crystal color lines on the test plate are nearly linear in the transverse direction normal to the flow stream along the plate, indicating that the two-dimensional jet flow attaches upon the plate.

3. Data reduction

Details of the flow and heat transfer measurement technique used in this study are described by Yoon et al. [5] and Lee et al. [10], respectively. For flow field measurements in the OWAOJ, a split film probe (TSI-1288) which is an end-flow-type, 0.15 mm diameter and 2 mm long, is used. This probe is calibrated at the exit of the round jet issuing from the nozzle of TSI-1125 calibrator. The probe calibration method used is the same as that described by Yoon et al. [5]. A location of the reattachment point is estimated by the forward flow fraction, γ_W, which is defined as the fraction of time duration during which the flow is directed towards downstream.

The streamwise and crosswise mean velocity components in the OWAOJ are measured using a constant temperature anemometer (TSI, IFA300). The initial turbulence intensities at the nozzle exit are $u'/U_J = 0.7\%$, $v'/U_J = 0.5\%$ and $w'/U_J = 0.6\%$, respectively. A calibrated 0.025 cm diameter chromel–alumel thermocouple measures the jet exit temperature to an accuracy of $\pm 0.1^{\circ}$C.

By electrically heating a gold-coating on the Intrex, an essentially uniform wall heat flux condition is established. The heat flux can be adjusted by changing the current through the Intrex, which changes the surface temperature. Under the uniform heat flux boundary condition, an isotherm on the Intrex surface corresponds to a contour of uniform heat transfer coefficient. As the heat flux on the Intrex changes, the position of the particular color being observed also changes. And the local heat transfer coefficient at that position is calculated from

$$h = \frac{q_v}{(T_W - T_J)} \tag{1}$$

where T_W is the plate surface temperature measured by liquid crystal, T_J is the jet temperature, q_v is the convection heat flux which is obtained by subtracting the radiation and conduction heat losses from the total heat flux through the Intrex, i.e.

Table 1
Nusselt number uncertainty analysis

X_1	Value	δx_i	$\frac{\delta x_i \partial Nu}{Nu \partial x_i}$ (%)
T_W (°C)	35.23	0.20	3.233
f	1.0	0.02	2.453
T_J (°C)	27.83	0.14	2.02
ε	0.9	0.05	0.742
I (A)	0.761	0.0016	0.253
T_a (°C)	27.20	0.14	0.224
D (m)	0.025	5.0×10^{-5}	0.214
V (V)	66.91	0.034	0.061
A (m^2)	0.12	5.6×10^{-5}	0.056
Total Nu uncertainty: $\frac{\delta Nu}{Nu} = 4.61\%$			

$$q_v = \frac{fIV}{A} - \varepsilon\sigma\ T_W^4 - T_a^4 c) - q \tag{2}$$

The ratio of the local electrical heating to the average heating, f, is a measure of the uniformity of the gold-coating. It turns out that the gold-coating uniformity is as high as 98% when the test section of the Intrex is small and selected from the middle of a roll where the gold-coating is most uniform. Therefore, we assume $f \approx 1$ for the heat flux calculation. But f is maintained in Eq. (2) because it contributes to the overall uncertainty (see Table 1).

The Nusselt number uncertainty analysis on the basis of 20:1 odds (i.e., 95% confidence level of errors) has been carried out using the method by Kline and Mcklintock [11]. Table 1 shows that the Nusselt number uncertainty for $H/D = 2.5$, $\alpha = 10^\circ$, and $X^\alpha/D = 2$ at $Re = 17{,}700$ is estimated to be 4.61%. It should be noted that this uncertainty represents the maximum uncertainty in the Nusselt number under the given experimental conditions. The uncertainty due to a surface temperature measurement by liquid crystal is the largest contribution to the overall Nusselt number uncertainty. Another important source of uncertainty is the gold-coating uniformity on the Intrex surface. The uncertainty analysis also shows that the uncertainty in the mean velocity is less than 5%.

4. Results and discussion

4.1. Flow characteristics

The distributions of the wall static pressure coefficient along the plate are shown in Fig. 2 for $Re = 53{,}200$, $H/D = 5$, and $\alpha = 0^\circ$ to 40°. The wall static pressure coefficient is defined as

$$c_{P_W} = \frac{(P_W - P_\infty)}{1/2\rho U_J^2} \tag{3}$$

where, P_W, P_∞, ρ, and U_J are the wall static pressure on the plate surface, atmospheric pressure, air density, and jet mean velocity at the nozzle exit.

In general, Fig. 2 shows that when a two-dimensional slot jet is issued into quiescent surroundings above an inclined plate, the so-called "coanda effect", caused by a difference in the flow entrainment across the jet, forces the jet to deflect towards the wall boundary, reattach to the plate surface, and redevelop along the plate, creating three distinct flow regions (recirculation, impingement or reattachment, and wall jet) as shown in Fig. 1. The static pressure along the plate wall, on the other hand, gradually decreases and approaches to a minimum value in the recirculation region. However the wall static pressure sharply rises to a maximum value near the reattachment point as the jet flow impinges upon the plate wall and gradually approaches to an atmospheric pressure in the wall jet region. The pressure distribution for $H/D = 4.0$, $\alpha = 0^\circ$, and $Re = 15500$ by Borque and Newmann [1] is also plotted in Fig. 2, which is in qualitative agreement with those of the present results.

It is observed from Fig. 2 that as the oblique angle α increases from 0° to 40°, the point of the maximum wall pressure coefficient on the plate surface progressively shifts downstream and its magnitude decreases. The minimum wall pressure point also shifts downstream with an increasing oblique angle, but its magnitude remains nearly unchanged. It is also observed that with an increasing oblique angle, slopes in the pressure rise become shallower after the minimum pressure point and an approach to the atmospheric pressure thereafter slower past the maximum pressure point.

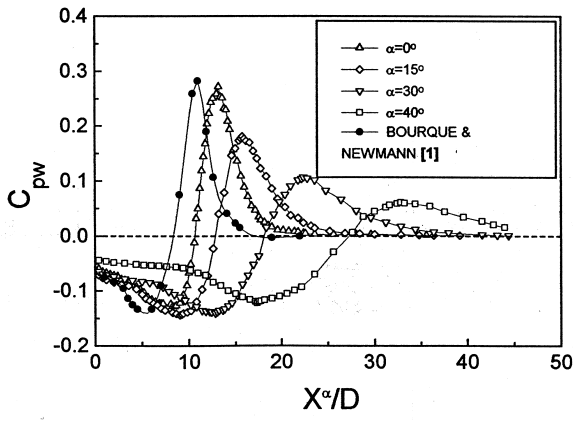

Fig. 2. Distributions of the wall static pressure coefficient for various α at $H/D = 5.0$ and $Re = 53{,}200$.

In particular, in the case of the largest oblique angle ($\alpha = 40^\circ$) tested, the magnitude of the wall pressure coefficient remains nearly the same up to one half of the minimum pressure position. It may be attributed to the fact that the large oblique angle enables a large amount of the flow entrainment as the jet discharges. The same flow behaviors described above were also observed for other H/D's tested, but are not presented here due to a space limit.

Fig. 3 shows variations of the reattachment length, X^{α}_{R}, the maximum Nusselt number position, $X^{\alpha}_{Nu_{max}}$, and the maximum wall pressure position, $X^{\alpha}_{cp_{max}}$, with the offset ratio, H/D for $Re = 53{,}200$ and $\alpha = 0^\circ$ to 40°. The reattachment length has been used as an important parameter to better understand the flow characteristics of the WAOJ. According to our previous WAOJ research results [9], the WAOJ flow reattachment is a very unsteady process, resulting in a wide reattachment region. In spite of the unsteadiness of the reattachment region, Kim et al. [9] defined the reattachment length as the time-averaged reattachment point of the unsteady reattaching flow. It coincides with the point where the mean skin friction coefficient vanishes (i.e., the γ_W value becomes 0.5). They showed that the reattachment length increases with an increasing offset ratio. Similar flow behaviors can be expected for the OWAOJ since the WAOJ is a limiting case of the OWAOJ for ($\alpha = 0^\circ$).

It is shown from Fig. 3 that the reattachment length increases with an increasing offset ratio and oblique angle. The reattachment length for the case of $\alpha = 0^\circ$ in the present experiment is in a good agreement with those of Borque and Newmann [1], and Hoch and Jiji [3]. Fig. 3 also shows the position of the time-averaged reattachment point nearly coincides with the maximum Nusselt number position for all oblique angles tested. Vogel and Eaton [12], and Baughn et al. [13] have demonstrated in the backward-facing step flow and in the round abrupt expansion flow, respectively, that the maximum Nusselt number position closely agrees with the reattachment point, and in the light of the close similarity of the flows, it can be assumed that the same is true for the OWAOJ. It is worthy to note that for a given offset ratio and Reynolds number, there seems to exist a critical oblique angle at which the flow reattachment can occur. For $Re = 53{,}200$, the critical oblique angles are as follows: $\alpha_{cr} = 59^\circ$, 57°, 55°, 52° and 50° for $H/D = 0$, 2.5, 5.0, 7.5 and 10, respectively.

It should also be noted from Fig. 3 that the reattachment point nearly coincides with the maximum wall pressure position for $\alpha = 0^\circ$. However, as the oblique angle increases from $\alpha = 0^\circ$, gap between the reattachment point and the maximum wall pressure position becomes larger. It turns out that for $\alpha \geq 30^\circ$, the reattachment point coincides more closely with the point where the pressure coefficient changes from the negative to the positive value than with the maximum pressure position. Fig. 4 shows the effect of the oblique angle on the reattachment length, X^{α}_{R} and maximum wall pressure position, $X^{\alpha}_{cp_{max}}$ for $Re = 53{,}200$ and that they are well correlated by the following expressions:

$$X^{\alpha}_{R}/D = 4.854(H/D)^{0.6}(\cos\alpha)^{-3.02} \tag{4}$$

and

$$X^{\alpha}_{cp_{max}}/D = 4.975(H/D)^{0.6}(\cos\alpha)^{-3.52} \tag{5}$$

According to Eqs. (4) and (5), X^{α}_{R} has the same dependency on the offset ratio (i.e., $(H/D)^{0.6}$) as $X^{\alpha}_{cp_{max}}$. However, $X^{\alpha}_{cp_{max}}$ is more dependent upon the oblique angle than X^{α}_{R}. The above correlations are valid for $2.5 \leq H/D \leq 10$, $0^\circ \leq \alpha \leq 40^\circ$, and $Re = 53{,}200$.

The mean velocity vector profiles in the initial flow

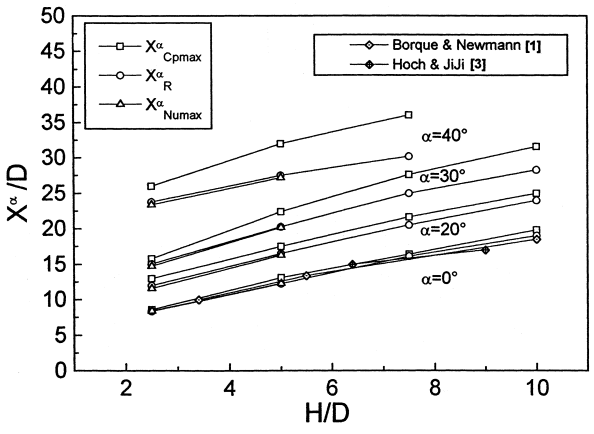

Fig. 3. Variations of the reattachment length, maximum Nusselt number position, and maximum wall pressure position with H/D for various α and $Re = 53{,}200$.

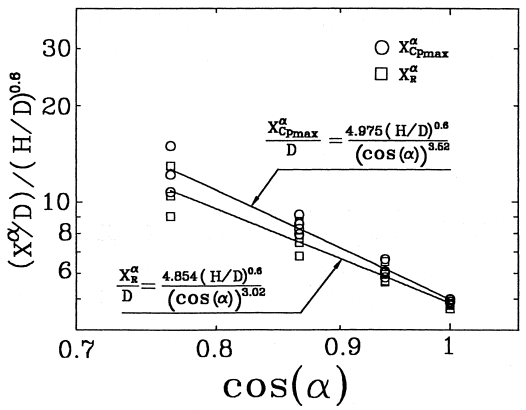

Fig. 4. Effect of the oblique angle on the reattachment length and maximum pressure position for $Re = 53{,}200$.

development region of the OWAOJ for $H/D = 5$ and $\alpha = 0^\circ$, 20°, and 40° are shown in Fig. 5(a)–(c). From Fig. 5(a) and (b), the recirculation region is readily observed with the vortex center located at $X/D \approx 7$ and $X^\alpha/D \approx 9$ for $\alpha = 0^\circ$ and 20°, respectively. The primary jet flow appears to gradually curve through the first one-third of the recirculation region and turns sharply downward as the jet impinges on the plate. This trend has also been observed in the backward facing step flows [12], but the streamline started to curve after one-half of the recirculation bubble. In the present experiment, the maximum reverse flow velocities for $\alpha = 0^\circ$ and 20° are about 33 and 26%, respectively, of the jet exit velocity. On the other hand, for $\alpha = 40^\circ$, the mean velocity vector profile in Fig. 5(c) resembles a free jet flow with a weak flow reversal near the plate wall, suggesting that the flow nearly departs from the WAOJ. The consistent flow behavior is also demonstrated in Fig. 7 and Fig. 8 later.

To investigate the flow characteristics of the

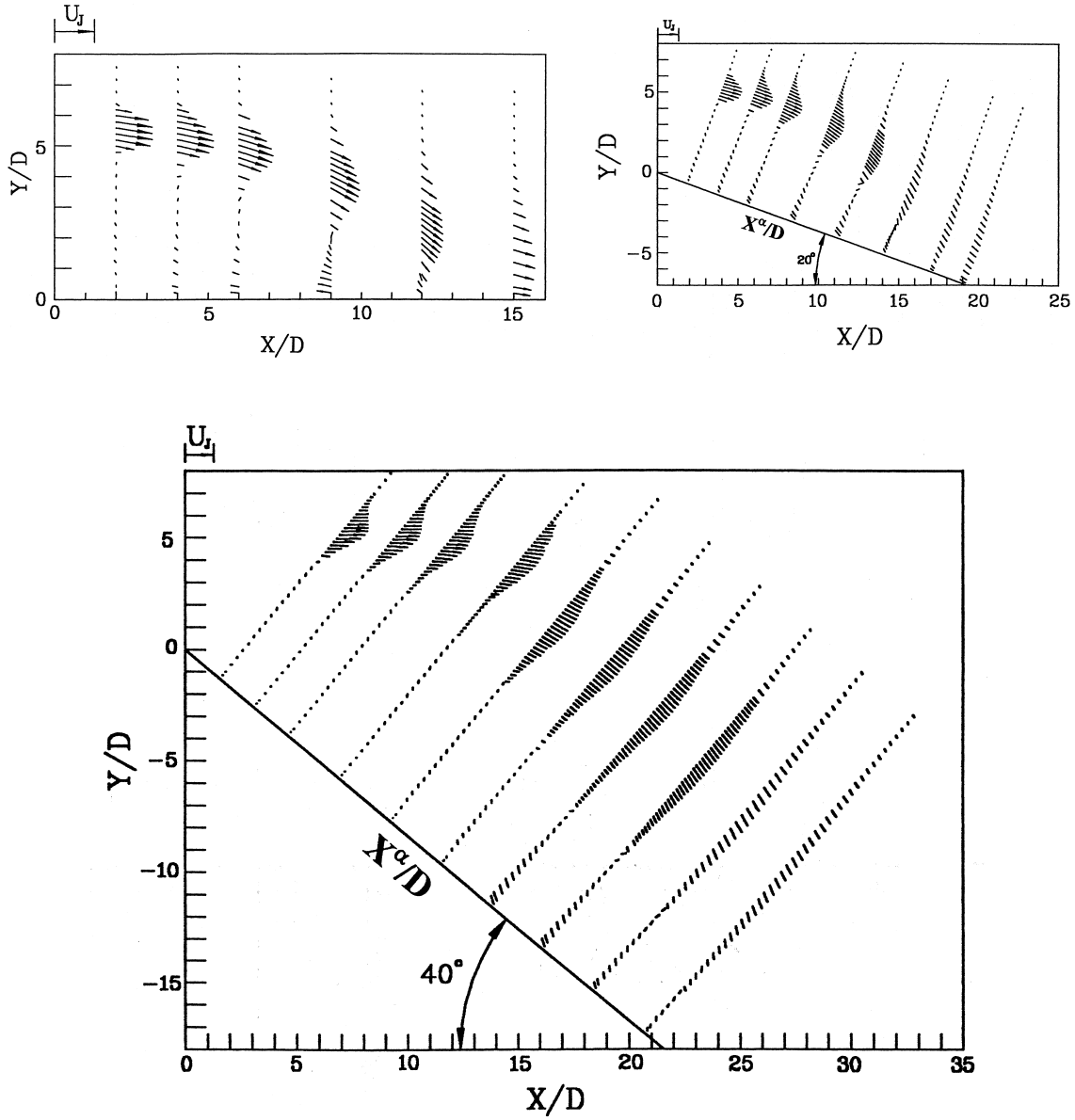

Fig. 5. (a) Mean velocity vector profiles for $\alpha = 0^\circ$ at $H/D = 5.0$ and $Re = 53{,}200$. (b) Mean velocity vector profiles for $\alpha = 20^\circ$ at $H/D = 5.0$ and $Re = 53{,}200$. (c) Mean velocity vector profiles for $\alpha = 40^\circ$ at $H/D = 5.0$ and $Re = 53{,}200$.

OWAOJ in the far downstream region, the mean velocity distributions for different oblique angles are plotted along the vertical distance in Fig. 6. The solid line in Fig. 6 represents the velocity profile for the fully developed plane wall jet (PWJ), investigated by Schwarz and Cosart [14]. According to both Rajaratnam and Subramanya [15] and Kim et al. [9] who performed the PWJ and WAOJ experiments, respectively, the mean velocity profiles show a similarity in the wall jet region corresponding to $X^{\alpha} \geq 20D$. The same flow behavior can be observed for $\alpha = 0^{\circ}$ in Fig. 6. However, as the oblique angle increases, the starting position of the velocity similarity moves further downstream (i.e., $X^{\alpha} = 30D$ for $\alpha = 20^{\circ}$ and $X^{\alpha} = 40D$ for $\alpha = 30^{\circ}$) and for $\alpha = 40^{\circ}$, the velocity similarity would not be observed until $X^{\alpha} = 50D$.

The axial turbulence intensity profiles for $H/D = 5$, $Re = 53{,}200$ and $\alpha = 0^{\circ}$ to 40° are shown in Fig. 7. The turbulence intensity distributions measured by Irwin [16] at $X/D = 194$ in a self-preserving plane wall jet are also plotted to compare with the present results. Both results show that the axial turbulence intensity profiles in the WAOJ nearly attain their self-preserving state at $X^{\alpha} \approx 30D$ for $\alpha \leq 20^{\circ}$, and $X^{\alpha} \approx 40D$ and 50D for $\alpha = 30^{\circ}$ and 40°, respectively. This behavior is consistent with the axial mean velocity results.

The logarithmic plots of the maximum axial velocity distributions for $H/D = 5$, $Re = 53{,}200$ and $\alpha = 0^{\circ}$ to 40° are shown in Fig. 8. Within the experimental uncertainty, it follows that for $\alpha = 0^{\circ}$ to 30°, the maximum velocity decay of the OWAOJ in the wall jet region obeys the conventional $-1/2$ power law of the WAOJ (i.e., $U_{\mathrm{m}} \propto 1/\sqrt{x^{\alpha}}$). The maximum axial velocity distributions for $H/D = 5.7$ and $\alpha = 0^{\circ}$ by Hoch and Jiji [3] also show the same velocity decay as the present results. However, for $\alpha = 40^{\circ}$, the maximum velocity decay profile appears to deviate from the typical fully-developed WAOJ. Thus, it can be concluded that when the oblique angle is greater than 40°, the flow may very much depart from the WAOJ.

4.2. Heat transfer characteristics

The local Nusselt number distributions along the plate are presented in Fig. 9 for two offset ratios, one Reynolds number of $Re = 53{,}200$, and five oblique angles. In general, the positions and magnitudes of the maximum Nusselt number are much influenced by oblique angle and offset ratio. It is observed from Fig. 9 that for larger offset ratio and increasing oblique angle, the difference in the entrainment rate along the inner and outer edges of the jet diminishes. This results in the weakening of the "coanda effect", which in turn causes the weaker jet impingement force on the plate and subsequent reduction in the Nusselt number magnitude.

It is also observed from both Figs. 5 and 9 that $Nu_{\max}$ position ($X^{\alpha}_{Nu_{\max}}$) increases with increasing oblique angle and offset ratio. The correlations between $Nu_{\max}$, oblique angle and offset ratio will be discussed shortly. The local Nusselt number in the recirculation region increases due to turbulent mixing processes by the recirculation bubble and reaches a maximum value at the point where the jet flow reattaches as demonstrated in Fig. 3. The Nusselt number in the wall jet region begins to decrease monotonically from the maximum value at the reattachment point and likely converges (except for $\alpha = 40^{\circ}$) to approximately the same value at $X^{\alpha}/D \approx 24$ and 30 for $H/D = 2.5$ and

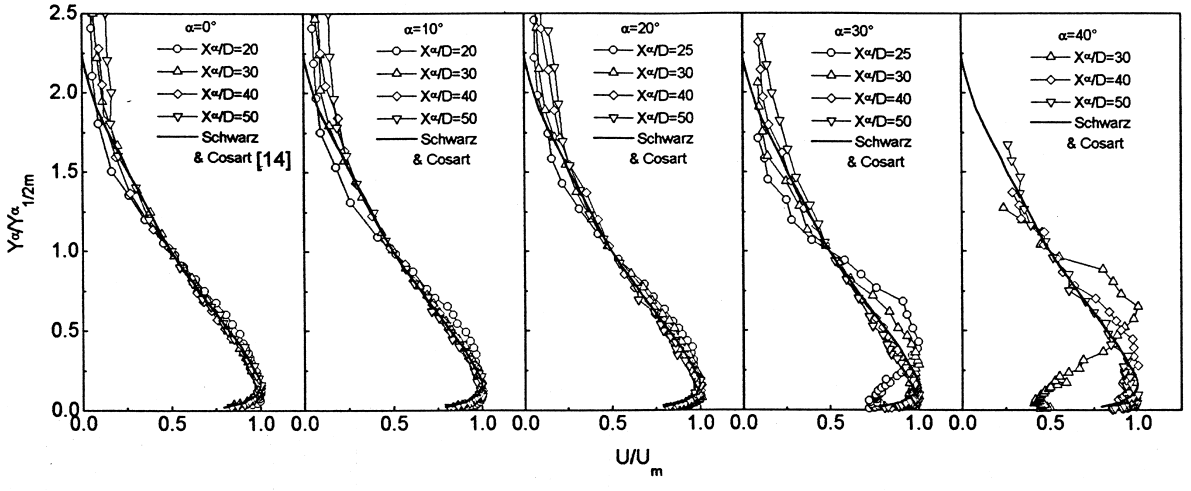

Fig. 6. Dimensionless axial mean velocity profiles for various α at $H/D = 5.0$ and $Re = 53{,}200$.

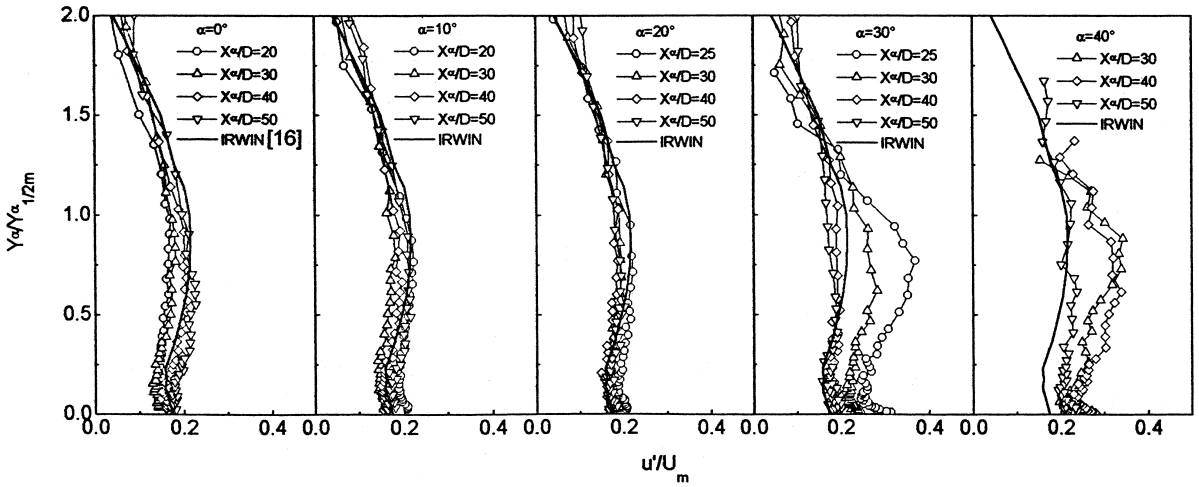

Fig. 7. Dimensionless axial turbulence intensity profiles for various α at $H/D = 5.0$ and $Re = 53{,}200$.

5.0. respectively, as the flow redevelops far downstream.

It should be noted from Fig. 9 that the minimum Nusselt number occurs between $X^{\alpha}/D \approx 1.0$ and $X^{\alpha}/D \approx 4.0$ for the offset ratios and oblique angles tested, with an increase of the Nusselt number as the upstream inclined wall is approached. This increase of the Nusselt number is attributed to an additional mixing of the flow caused by a secondary recirculation in the upstream corner near the step of the inclined wall. The existence of the secondary recirculation is also observed by the color display of liquid crystal on the plate wall.

Variations of the maximum Nusselt number, $Nu_{\max}$, with jet Reynolds number and oblique angle are shown in Fig. 10 for two offset ratios of $H/D = 2.5$ and 5.0. The maximum Nusselt number varies according to $Nu_{\max} \propto (Re)^{0.52-0.56}$ and $Nu_{\max} \propto (Re)^{0.52-0.65}$ for $H/D = 2.5$ and 5.0, respectively. The exponents to Reynolds number correspond to each oblique angle from $\alpha = 40^{\circ}$ to 0°. As shown in Fig. 3, the maximum Nusselt number position nearly coincides with the reattachment point and the reattachment point formed by the OWAOJ can be considered as the stagnation point in the impinging jet. The Reynolds number dependence of $Nu_{\max}$ is somewhat stronger for $H/D = 5.0$ than for $H/D = 2.5$. This may be due to an increase of turbulence in the approaching jet as a result

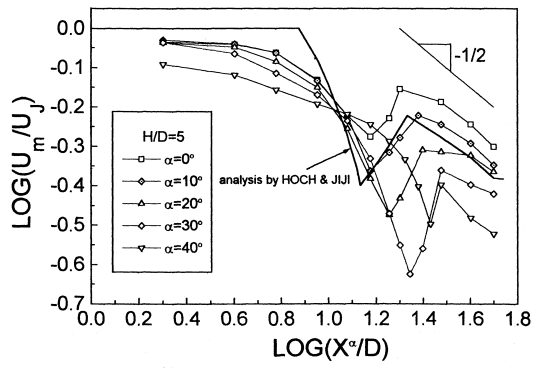

Fig. 8. Logarithmic plots of the maximum axial velocity distributions to show a $-1/2$ power law decay for various α at $H/D = 5.0$ and $Re = 53{,}200$.

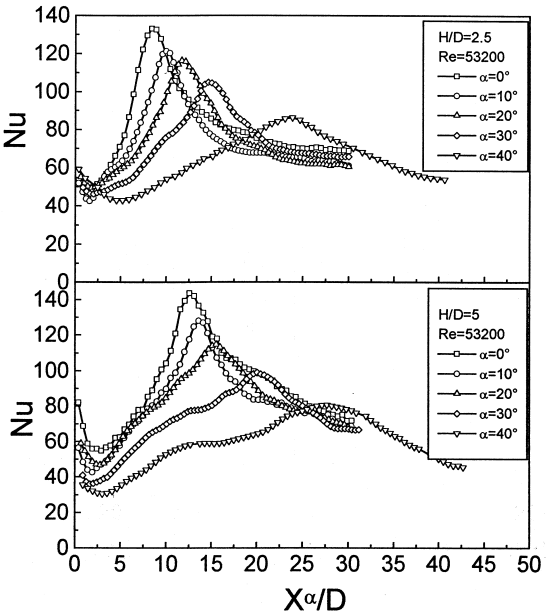

Fig. 9. Streamwise variations of the local Nusselt number with α and H/D at $Re = 53{,}200$.

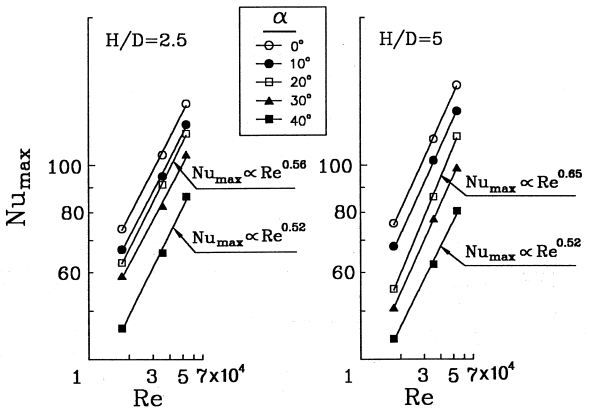

Fig. 10. Effect of Reynolds number on the maximum Nusselt number for $H/D = 2.5$ and 5.0.

of stronger exchange of momentum with surrounding air since for the larger offset ratio, the jet travels a longer distance before impinging on the plate. Our results are consistent with those of impinging jet flow studies by Lee et al. [17] and Hollworth and Gero [18] for which the exponents to Reynolds number varied from $n = 0.5$ to 0.67 depending on the nozzle-to-plate distances and Reynolds numbers tested. Kumada et al. [6] also reported in their mass transfer study with the WAOJ that the maximum Sherwood number depends on $Re^{0.58}$ for the offset ratios ranging from $H/D = 2.5$ to 24.5.

Fig. 11 shows variations of the mean Nusselt number with the oblique angle in the initial development region corresponding to $X^{\alpha} \leq 30D$. The mean Nusselt number is defined as

$$Nu_{\text{mean}} = \frac{1}{X^{\alpha}} \int_{o}^{X^{\alpha}} Nu \, \mathrm{d}X^{\alpha} \tag{6}$$

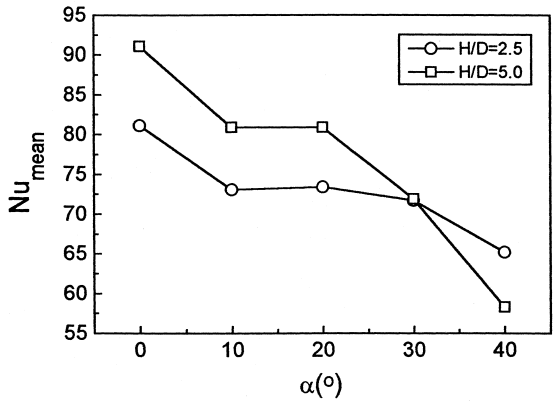

Fig. 11. Mean Nusselt number variations with α for $H/D = 2.5$ and 5.0 at $Re = 53{,}200$.

The results show that the largest Nu_{mean} occurs at $\alpha = 0^{\circ}$ for $H/D = 2.5$ and 5.0. The magnitude of Nu_{mean} is larger for $H/D = 5.0$ than that for $H/D = 2.5$ at $\alpha \leq 20^{\circ}$. This may be due to an increase of turbulence in the approaching jet as a result of stronger exchange of momentum with surrounding air. However, the magnitude of Nu_{mean} is larger for $H/D = 2.5$ than that for $H/D = 5.0$ at $\alpha = 40^{\circ}$, since for $H/D = 5.0$, the jet travels a longer distance before impinging on the plate. Consequently, the upper jet spread becomes wider and impinging effect is reduced.

5. Summary

Turbulent flow and heat transfer characteristics of a two-dimensional oblique wall attaching offset jet have been experimentally investigated. The following conclusions can be drawn:

1. As the oblique angle increases from $\alpha = 0^{\circ}$ to 40°, the point of the maximum wall pressure coefficient along the plate surface progressively shifts downstream and its magnitude decreases, while the minimum wall pressure point also shifts downstream with its magnitude remaining nearly unchanged. Slopes in the pressure rise becomes shallower with an increasing oblique angle after the minimum pressure point and an approach to the atmospheric pressure thereafter slower past the maximum pressure point.
2. The flow similarity in the wall jet region is observed for $X^{\alpha} \geq 20D$ at $\alpha = 0^{\circ}$. But, as the oblique angle increases, the position of similarity moves further downstream, and for $\alpha = 40^{\circ}$, the flow similarity is not observed until $X^{\alpha} = 50D$. The decay of the maximum axial velocity in the OWAOJ obeys the $-1/2$ power law of the wall attaching offset jet for $\alpha \leq 30^{\circ}$.
3. The local Nusselt number in the recirculation region increases due to turbulent mixing processes by the recirculation bubble and reaches a maximum value at the reattachment point. The maximum Nusselt number varies according to $Nu_{\max} \propto (Re)^{0.52-0.56}$ and $Nu_{\max} \propto (Re)^{0.52-0.65}$ for $H/D = 2.5$ and 5.0, respectively.
4. The maximum Nusselt number point nearly coincides with the time-averaged reattachment point for all oblique angles tested and the maximum pressure position for $\alpha < 20^{\circ}$.
5. The minimum Nusselt number occurs between $X^{\alpha}/D \approx 1.0$ and $X^{\alpha}/D \approx 4.0$ for all H/D's and α's tested, with an increase of the Nusselt number as the upstream inclined wall is approached. This increase of the Nusselt number is due to an ad-

ditional mixing caused by the secondary recirculation.

References

[1] C. Borque, G. Newmann, Reattachment of a two-dimensional incompressible jet to an adjacent flat plate, Aerion Quat 11 (1960) 201–232.

[2] R.A. Sawyer, Two-dimensional reattachment jet flows including the effect of curvature on entertainment, J. Fluid Mech 17 (1963) 481–498.

[3] J. Hoch, M. Jiji, Two-dimensional turbulent offset jet boundary interaction, J. Fluids Engng 103 (1981) 154–161.

[4] J.R.R. Pelfray, J.A. Liburdy, Mean flow characteristics of a turbulent offset jet, J. Fluids Engng 108 (1986) 82–88.

[5] S.H. Yoon, K.C. Kim, D.S. Kim, M.K. Chung, Comparative study of a turbulent wall-attaching offset jet and a plane wall jet, Trans. KSME J 7 (1993) 101–112.

[6] M. Kumada, I. Mabuchi, K. Oyakawa, Studies in heat transfer to turbulent jets with adjacent boundaries (3rd report: mass transfer to plane turbulent jet reattachment on an offset parallel plate), Bull. JSME 16 (1973) 1712–1722.

[7] J. Hoch, M. Jiji, Theoretical and experimental temperature distribution in two-dimensional turbulent jet boundary interaction, J. Heat Transfer 103 (1981) 331–336.

[8] J.T. Holland, J.A. Liburdy, Measurements of the thermal characteristics of heated offset jet, Int. J. Heat Mass Transfer 33 (1990) 69–78.

[9] D.S. Kim, S.H. Yoon, D.H. Lee, K.C. Kim, Flow and heat transfer measurements of a wall attaching offset jet, Int. J. Heat Mass Transfer 39 (1996) 2907–2913.

[10] S.J. Lee, J.H. Lee, D.H. Lee, Local heat transfer measurements from an elliptic jet impinging on a flat plate using liquid crystal, Int. J. Heat Mass Transfer 37 (1994) 967–976.

[11] S.J. Kline, F.A. McKlintock, Describing uncertainties in single sample experiments, Mech. Engng 5 (1953) 3–8.

[12] J.C. Vogel, J.K. Eaton, Combined heat transfer and fluid dynamic measurements downstream of a backward-facing step, J. of Heat Transfer 107 (1985) 922–929.

[13] J.W. Baughn, S. Shimizu, Heat transfer measurements from a surface with uniform heat flux and an impinging jet, J. of Heat Transfer 111 (1989) 1096–1098.

[14] W.H. Schwarz, W.P. Cosart, The two-dimensional turbulent wall jet, J. Fluid Mech 10 (1961) 481–495.

[15] N. Rajaratnam, N. Subramanya, Plane turbulent reattached wall jet, J. Hydraulic Div 94 (1968) 95–112.

[16] H.P.A.H. Irwin, Measurements in a self-preserving plane wall jet in a positive pressure gradient, J. Fluid Mech 61 (1) (1973) 33–63.

[17] D.H. Lee, R. Greif, S.J. Lee, J.H. Lee, Heat transfer from a flat plate to a fully developed axisymmetric impinging jet, J. of Heat Transfer 117 (1995) 772–776.

[18] B.R. Hollworth, L.R. Gero, Entrainment effects on impingement heat transfer. Part 2: local heat transfer measurements, J. of Heat Transfer 107 (1985) 910–915.